HEAT AND MASS TRANSFER ANALYSIS ON MHD BLOOD FLOW OF CASSON FLUID MODEL DUE TO PERISTALTIC WAVE

by

Mohammad M. RASHIDI[a,b], Zhigang YANG[a,b], Muhammad M. BHATTI[c*], and Munawwar Ali ABBAS[d,**]

[a] Shanghai Key Laboratory of Vehicle Aerodynamics and Vehicle Thermal Management Systems, Tongji University, Shanghai, China
[b] ENN-Tongji Clean Energy Institute of Advanced Studies, Shanghai, China
[c] Shanghai Institute of Applied Mathematics and Mechanics, Shanghai University, Shanghai, China
[d] Department of Mathematics, Shanghai University, Shanghai, China

Original scientific paper
https://doi.org/10.2298/TSCI160102287R

In this article, heat and mass transfer analysis on MHD blood flow of Casson fluid model due to peristaltic wave has been investigated. The governing equations of blood flow for Casson fluid model, temperature, and energy equation have been solved by taking the assumption of long wavelength and neglecting the inertial forces. The resulting coupled differential equations have been solved analytically and the exact solutions are presented. The impact of various pertinent parameters is plotted and discussed. It is found that the influence of magnetic field and fluid parameter shows similar behavior on velocity profile while its behavior is opposite for pressure rise and pressure gradient profile. Trapping phenomena have also taken into account by sketching the streamlines. The expression for pressure rise and friction forces are evaluated numerically.

Key words: *MHD, Casson fluid, heat and mass transfer, blood flow*

Introduction

Blood flow problems have received a major attention by various researchers during the past few years. Blood in the human body carries out various types of functions like transport of nutrients and oxygen for their metabolic activity, removal of carbon dioxide, removal of metabolic products and circulation. Furthermore, micro-circulation in a human body is very much helpful to maintain the body temperature stable. The rheological feature of blood such as non-Newtonian viscosity, viscoelasticity, physicochemical features of plasma and thixotropy play a major role in flow regulation in various diseases and health. Blood is composed of red blood cells (RBC), white blood cells (WBC) and platelets. Srivastava and Saxena [1] investigated two layered Casson fluid model through stenotic vessels which are applicable to the cardiovascular system. Later, Srivastava [2] explored the particle fluid suspension model of blood flow through stenotic vessels. Again, Srivastava and Saxena [3] described the two-fluid model for non-Newtonian blood induced by the peristaltic wave. Several authors [4-10] examined the blood flow problems with various biological fluids.

* Corresponding author, e-mail: muhammad09@shu.edu.cn, mubashirme@yahoo.com
** Now at: Department of Computer Science, University of Baltistan, Skardu, Pakistan

The peristaltic mechanism is a spontaneous process that occurs due to symmetrical contraction and suspension of smooth muscles in a living body. In a human body, urine transport from a kidney to the bladder, gastrointestinal tract, ovum in the female fallopian tube, male and female reproductive systems are the most common examples in which peristaltic waves occurs. Many devices work on the mechanism of peristalsis *e. g.* finger pumps, dialysis machine, blood pump machines, and roller pumps. Bio-heat transfer has also received a major attention due to its wide application in thermoregulation and human thermotherapy system. Peristaltic flow with heat and mass transfer has also various applications in biomedical engineering, physiology, and nuclear industry like conduction process in tissues, vasodilation, convection of heat due to blood flow, radiation between a surface and its environment, and processing of various food items. Peristaltic flow with heat and mass transfer can also be observed in oxygenation and hemodialysis. The mass transfer also plays an important and significant role in a human body such as diffusion process. Mass transfer is also applicable in a various industrial process such as reversal osmosis, combustion process, diffusion of chemical properties, and membrane separation process. Akbar [11] analyzed the effects of heat and mass transfer on Carreau blood flow model through a tapered stenosis artery. Akbar *et al.* [12] examined the heat transfer analysis on a metachronal wave of cilia in copper nanofluids. Nadeem *et al.* [13] studied the nanoparticle phenomena on peristaltic flow of Jeffrey fluid model through a rectangular duct. Ellahi *et al.* [14] considered the effects of heat and mass transfer on peristaltic flow of viscous fluid in a non-uniform rectangular duct. Extensive literature on the present analysis can be found from the references [15-20] and several therein.

On the other hand, MHD also play a major and important role in biomedical engineering such as it is very helpful in magnetic drug targeting for various types of cancer diseases. MHD is also found in various engineering problems like electromagnetic casting, cooling of different nuclear reactors and plasma confinement. For various biological fluids, MHD is also favorable to control the flow due to the effects of Lorentz force. Mekheimer [21] explored the effects of magnetic field on peristaltic flow of couple stress fluid. Mekheimer *et al.* [22] considered the effects of magnetic field on peristaltic flow through a porous medium due to a surface acoustic wavy wall. Rashidi *et al.* [23] analyzed numerically the influence of magnetic field and heat transfer on nanofluid in a channel having sinusoidal walls. Sheikholeslami *et al.* [24] investigated the effects of magnetic field and heat transfer on nanofluid using two phase model. According to best of my knowledge, heat and mass transfer analysis of MHD blood flow of Casson fluid model due to peristaltic wave has not yet been reported.

With the above analysis in mind, the main objective of this present investigation is to analyze the effects of heat and mass transfer on MHD blood flow of Casson fluid model due to peristaltic wave. The governing blood flow model is based on continuity, momentum, energy and concentration equations. These equations are simplified by taking the assumption of long wavelength and creeping flow regime. The solution of the resulting coupled differential equations have been obtained analytically and a closed-form solution is presented. The impact of all the physical parameters is demonstrated graphically and mathematically.

Mathematical formulation

Let us consider the peristaltic motion of Casson fluid (treated as blood) through a 2-D non-uniform channel with sinusoidal wave propagating towards down its walls. The fluid is electrically conducting by an external magnetic field B_0 applied to it. We have chosen Cartesian co-ordinate system in such a way that $\tilde{x}$-axis is considered along the center line in the

direction of wave propagation and ỹ-axis is transverse to it as shown in fig. (1). The geometry of the wall surface can be written:

$$\hbar(\tilde{x},\tilde{t}) = b(\tilde{x}) + \tilde{a}\sin\frac{2\pi}{\lambda\%}(\tilde{x} - \mathcal{C}\tilde{t}) \tag{1}$$

where

$$b(\tilde{x}) = b_0 + \mathcal{K}\tilde{x} \tag{2}$$

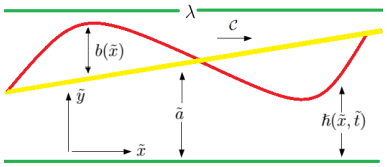

Figure 1. Geometry of the flow problem

The governing equation of continuity, momentum, energy, and concentration equation for incompressible, irrotational blood flow can be written:

$$\frac{\partial\tilde{u}}{\partial\tilde{x}} + \frac{\partial\tilde{v}}{\partial\tilde{y}} = 0 \tag{3}$$

$$\rho\left(\frac{\partial\tilde{u}}{\partial\tilde{t}} + \tilde{u}\frac{\partial\tilde{u}}{\partial\tilde{x}} + \tilde{v}\frac{\partial\tilde{u}}{\partial\tilde{y}}\right) + \frac{\partial\tilde{p}}{\partial\tilde{x}} = \mu\left(\frac{\partial S_{\tilde{x}\tilde{x}}}{\partial\tilde{x}} + \%\frac{\partial S_{\tilde{x}\tilde{y}}}{\partial\tilde{y}}\right) - \sigma B_0^2\tilde{u} \tag{4}$$

$$\rho\left(\frac{\partial\tilde{v}}{\partial\tilde{t}} + \tilde{u}\frac{\partial\tilde{v}}{\partial\tilde{x}} + \tilde{v}\frac{\partial\tilde{v}}{\partial\tilde{y}}\right) + \frac{\partial\tilde{p}}{\partial\tilde{y}} = \mu\left(\frac{\partial S_{\tilde{y}\tilde{x}}}{\partial\tilde{x}} + \frac{\partial S_{\tilde{y}\tilde{y}}}{\partial\tilde{y}}\right) \tag{5}$$

$$\zeta_0\left(\frac{\partial T}{\partial\tilde{t}} + \tilde{u}\frac{\partial T}{\partial\tilde{x}} + \tilde{v}\frac{\partial T}{\partial\tilde{y}}\right) = \frac{k}{\rho}\left(\frac{\partial^2 T}{\partial\tilde{x}^2} + \frac{\partial^2 T}{\partial\tilde{y}^2}\right) + \nu S_{\tilde{x}\tilde{y}}\left(\frac{\partial\tilde{u}}{\partial\tilde{y}}\right) \tag{6}$$

$$\left(\frac{\partial F}{\partial\tilde{t}} + \tilde{u}\frac{\partial F}{\partial\tilde{x}} + \tilde{v}\frac{\partial F}{\partial\tilde{y}}\right) = \mathcal{D}\left(\frac{\partial^2 F}{\partial\tilde{x}^2} + \frac{\partial^2 F}{\partial\tilde{y}^2}\right) + \frac{\mathcal{D}K_T}{T_m}\left(\frac{\partial^2 T}{\partial\tilde{x}^2} + \frac{\partial^2 T}{\partial\tilde{y}^2}\right) \tag{7}$$

The stress tensor for the Casson fluid model is defined:

$$\begin{aligned}\mathbf{S}^{1/n} &= \mathbf{S}_0^{1/n} + \mu\dot{\gamma}^{1/n},\\ \mathbf{S}_{i,j} &= 2E_{i,j}\left(\mu_b + \frac{\sqrt{2\pi_D}}{P_y}\right)\end{aligned} \tag{8}$$

In the previous equation $\pi = E_{i,j}$, and we have considered $P_y = 0$. Now, it is convenient to define the non-dimensional quantities:

$$x = \frac{\tilde{x}}{\lambda},\quad y = \frac{\tilde{y}}{b_0},\quad t = \frac{\mathcal{C}\tilde{t}}{\lambda},\quad u = \frac{\tilde{u}}{\mathcal{C}},\quad v = \frac{\tilde{v}}{\mathcal{C}\delta},\quad p = \frac{\tilde{p}b_0^2}{\mu\lambda\mathcal{C}},\quad h = \frac{\hbar}{b_0},\quad \phi = \frac{\tilde{a}}{b_0},\quad \nu = \frac{\mu}{\rho},$$

$$\mathrm{Re} = \frac{\rho\mathcal{C}b_0}{\mu},\quad \mathbf{S} = \frac{b_0}{\mu\mathcal{C}}\tilde{\mathbf{S}},\quad \delta = \frac{b_0}{\lambda},\quad \beta = \frac{\bar{\beta}_0}{b_0},\quad \mathrm{M} = B_0 b_0\sqrt{\frac{\sigma}{\mu}},\quad \mathrm{Sc} = \frac{\mu}{\rho\mathcal{D}},\quad \mathrm{Pr} = \frac{\zeta_0\rho\nu}{\kappa}, \tag{9}$$

$$\mathrm{Ec} = \frac{\mathcal{C}^2}{\zeta_0(T_1 - T_0)},\quad \mathrm{Sr} = \frac{\rho\mathcal{D}K_T(T_1 - T_0)}{\mu T_m(F_1 - F_0)}$$

Let us consider the assumption of long wavelength and creeping flow regime approximation. Using eq. (9) in eqs. (3)-(7), we get:

$$\frac{\partial p}{\partial x}=\left(1+\frac{1}{\zeta}\right)\frac{\partial^2 u}{\partial y^2}-\mathrm{M}^2 u \tag{10}$$

$$\frac{1}{\mathrm{Pr}}\frac{\partial^2\theta}{\partial y^2}=-\mathrm{Ec}\left(1+\frac{1}{\zeta}\right)\left(\frac{\partial u}{\partial y}\right)^2 \tag{11}$$

$$\frac{1}{\mathrm{Sc}}\frac{\partial^2 \Phi}{\partial y^2}+\mathrm{Sr}\frac{\partial^2\theta}{\partial y^2}=0 \tag{12}$$

subject to the respective no-slip boundary conditions:

$$\begin{gathered}\frac{\partial u}{\partial y}=0,\quad \theta(y)=\Phi(y)=0,\quad y=0\\ u(y)=0,\quad \theta(y)=\Phi(y)=1,\quad y=h=1+\frac{\mathcal{K}x\lambda}{b_0}+\phi\sin 2\pi(x-t)\end{gathered} \tag{13}$$

Solution of the problem

The exact solution of eqs. (10)-(12) can be obtained after integrating twice, we get:

$$u(y)=\frac{1}{\mathrm{M}^2}\frac{\mathrm{d}p}{\mathrm{d}x}\left(-1+\cosh \mathrm{M}y\sqrt{\frac{\zeta}{1+\zeta}}\ \mathrm{sech}\,\mathrm{M}h\sqrt{\frac{\zeta}{1+\zeta}}\right) \tag{14}$$

$$\begin{aligned}\theta(x,y)=&\frac{1}{8h\mathrm{M}^4\zeta\,\mathrm{sech}^2\mathrm{M}h\sqrt{\dfrac{\zeta}{1+\zeta}}}\left\{-\mathrm{Ec}\left(\frac{\mathrm{d}p}{\mathrm{d}x}\right)^2\mathrm{Pr}(h-y)\left[-1+(-1+2hM^2y)\zeta\right]+\right.\\ &+4\mathrm{M}^4y\zeta+\left[4\mathrm{M}^4\zeta-\mathrm{Ec}\left(\frac{\mathrm{d}p}{\mathrm{d}x}\right)^2(1+\zeta)\mathrm{Pr}\right]y\cosh 2h\mathrm{M}\sqrt{\frac{\zeta}{1+\zeta}}-\cosh 2\mathrm{M}y\sqrt{\frac{\zeta}{1+\zeta}}\cdot\\ &\left.\cdot\mathrm{Ec}\left(\frac{\mathrm{d}p}{\mathrm{d}x}\right)^2 h\mathrm{Pr}(1+\zeta)\right\}\end{aligned} \tag{15}$$

$$\begin{aligned}\Phi(x,y)=&\frac{1}{8h\mathrm{M}^4\zeta\,\mathrm{sech}^2\mathrm{M}h\sqrt{\dfrac{\zeta}{1+\zeta}}}\left\{\mathrm{Ec}\left(\frac{\mathrm{d}p}{\mathrm{d}x}\right)^2\mathrm{PrScSr}(h-y)\left[-1+(-1+2hM^2y)\zeta\right]+\right.\\ &+4\mathrm{M}^4y\zeta+\left[4\mathrm{M}^4\zeta-\mathrm{EcScSr}(1+\zeta)\left(\frac{\mathrm{d}p}{\mathrm{d}x}\right)^2\mathrm{Pr}\right]y\cosh 2h\mathrm{M}\sqrt{\frac{\zeta}{1+\zeta}}+\cosh 2\mathrm{M}y\sqrt{\frac{\zeta}{1+\zeta}}\cdot\\ &\left.\cdot\mathrm{PrScSrEc}h\left(\frac{\mathrm{d}p}{\mathrm{d}x}\right)^2(1+\zeta)\right\}\end{aligned} \tag{16}$$

The instantaneous volume rate is defined:

$$Q(x,t)=\int_0^h u\,\mathrm{d}y \tag{17}$$

The pressure gradient can be calculated with the help of previous equation, we get:

$$\frac{\mathrm{d}p}{\mathrm{d}x} = \frac{\mathrm{M}^3 Q\sqrt{\dfrac{\zeta}{1+\zeta}}}{-h\mathrm{M}\sqrt{\dfrac{\zeta}{1+\zeta}} + \tanh h\mathrm{M}\sqrt{\dfrac{\zeta}{1+\zeta}}} \tag{18}$$

The non-dimensional form of pressure rise, $\Delta \mathrm{P}_L$, and friction force, $\Delta \mathrm{F}_L$, at the wall along the whole length of the non-uniform channel, L, is given:

$$\Delta \mathrm{P}_L = \int_0^{L/\lambda} \left(\frac{\mathrm{d}p}{\mathrm{d}x}\right) \mathrm{d}x \tag{19}$$

$$\Delta \mathrm{F}_L = \int_0^{L/\lambda} -h\left(\frac{\mathrm{d}p}{\mathrm{d}x}\right) \mathrm{d}x \tag{20}$$

The expression for stream function satisfying equation of continuity are defined:

$$u = \frac{\partial \Psi}{\partial y}, \quad v = -\frac{\partial \Psi}{\partial x} \tag{21}$$

Special case: Newtonian fluid

The above results can be reduced to Newtonian fluid by taking $\zeta \to \infty$ in eq. (10) as a special case of our study. The solution of velocity profile for Newtonian fluid can be written:

$$u(y) = \frac{\dfrac{\mathrm{d}p}{\mathrm{d}x}\left(-1 + \cosh \mathrm{M}y \ \operatorname{sech} \mathrm{M}h\right)}{\mathrm{M}^2} \tag{22}$$

Numerical results and discussion

In this section the graphical results of all the physical parameters are sketched and discussed in detail. For this purpose figs. 2-10 have been sketched for velocity profile, pressure rise, friction forces, temperature profile, and concentration profile. The results for uniform channel can also be achieved by taking $\mathcal{K} \to 0$ in eq. (13). In eq. (14) by taking $\zeta \to \infty$, M = 0, the present results reduces to the results obtained by Shapiro *et al.* [5] and Srivastava and Srivastava [6] for power law index $n = 1$. Furthermore, the present results can also be obtained to the results obtained by Gupta and Seshadri [7] by taking $\zeta \to \infty$, M = 0 for a constant viscosity model. The expression of pressure rise and friction forces are evaluated numerically with the help of following parametric values: $\mathcal{K} = 5 \cdot 10^{-5}$, $L = \lambda = 10$ cm, $b_0 = 1 \cdot 10^{-2}$ cm, and the volume flow rate $Q(x, t)$ is periodic in $(x - t)$, *i. e.*:

$$Q = \bar{Q} + \phi \sin 2\pi(x - t)$$

where $\bar{Q}$ is the average volume flow rate. Figure (2) is plotted for velocity profile against Hartmann number, M, and Casson fluid parameter, ζ. From figs. 2(a) and 2(b), we can observe that when the Hartmann number and Casson fluid parameter increases then the velocity of the fluid increases near the wall, while its behavior start changing in the center of the channel and become opposite on the other wall. When the transverse magnetic field introduced in the flow then

Lorentz force generates which tends to resist the flow and results decrease in velocity profile. It depicts from fig. 3(a) that when the Hartmann number increases then the pressure rise increases and the maximum pressure is obtained in the center of the channel. It can be examined from fig. 3(b) that due to effect of Casson fluid parameter, ζ, pressure rise behaves as a decreasing function. It can be seen from fig. 4(a) and 4(b) that friction forces have completely opposite behavior as compared to pressure rise. Figures 5(a) and 5(b) is plotted for pressure gradient against multiple values of M and ζ. It can be observe from this figures that Hartmann number, M, significantly enhances the pressure gradient in the center of the channel whereas its behavior is converse against Casson fluid parameter, ζ, see fig. 5. It can be analyze from figs. 6(a) and 6(b) that when the Eckert number, Ec, and Prandtl number, Pr, increases then the temperature profile increases. We can also observe here that for large values of Prandtl number, thermal diffusivity dominates. It can be scrutinize from fig. 7(a) that due to the increment in the Schmidt number, the concentration profile decreases and the same behavior has been found for Soret number, Sr, as shown in fig. 7(b). It can be analyzed from figs. 8(a) and 8(b) that concentration also behaves as an decreasing function due to the effect of Eckert number and Prandtl number.

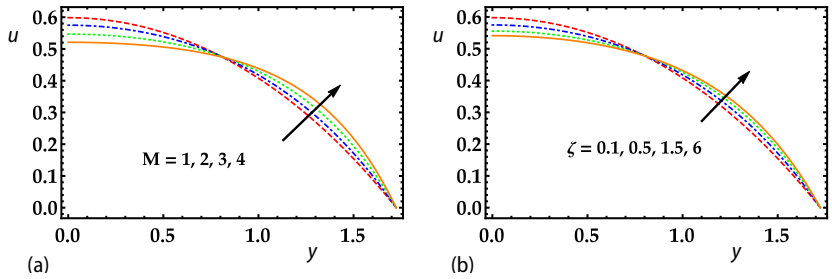

Figure 2. Velocity profile for different values of M and ζ, when $\varphi = 0.6$, $\bar{Q} = 0.1$

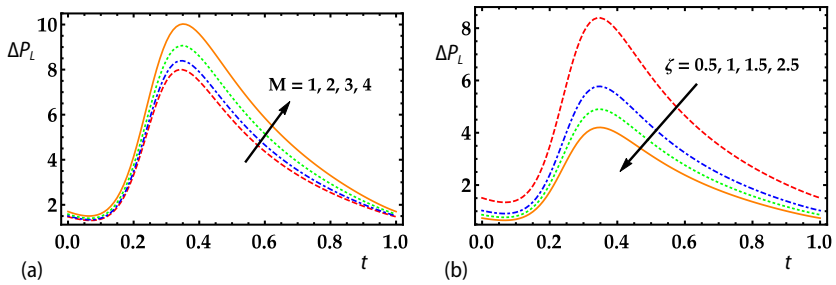

Figure 3. Pressure for different values of M and ζ, when $\varphi = 0.6$, $\bar{Q} = 0.1$

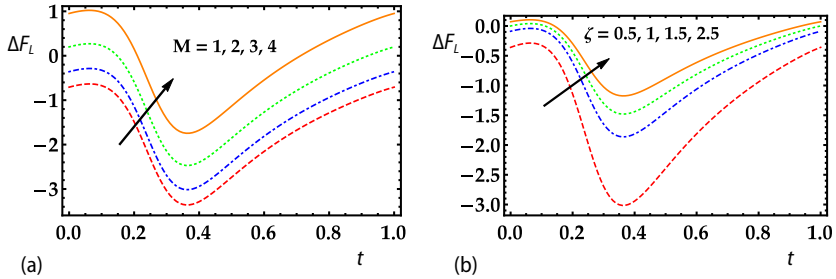

Figure 4. Friction force for different values of M and ζ, when $\varphi = 0.6$, $\bar{Q} = 0.1$

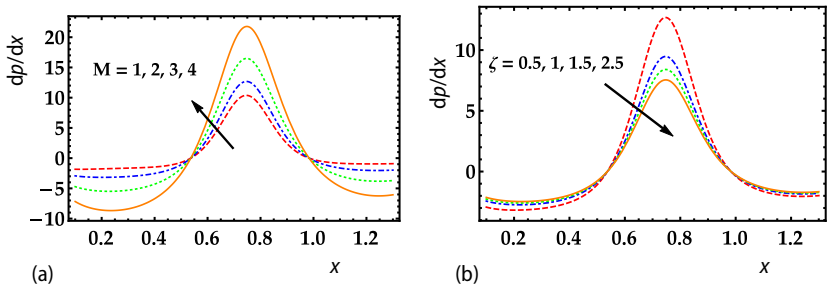

Figure 5. Pressure gradient for different values of M and ζ, when $\varphi = 0.6$, $\bar{Q} = 0.1$

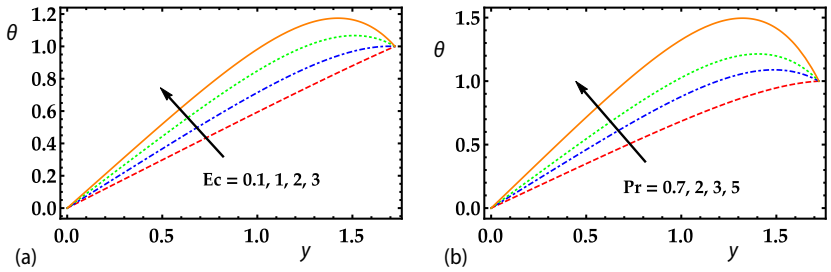

Figure 6. Temperature profile for different values of Ec and Pr, when $\zeta = 0.5$, $\varphi = 0.6$, $\bar{Q} = 0.1$, M = 2, Sc = 2, Sr = 2

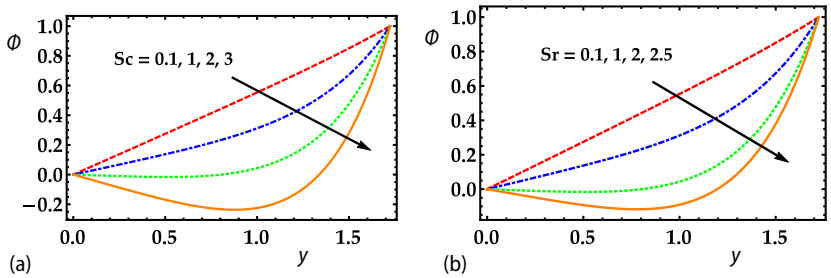

Figure 7. Concentration profile for different values of Sc and Sr, when $\zeta = 0.5$, $\varphi = 0.6$, $\bar{Q} = 0.1$, Ec = 1, Pr = 0.9, M = 2

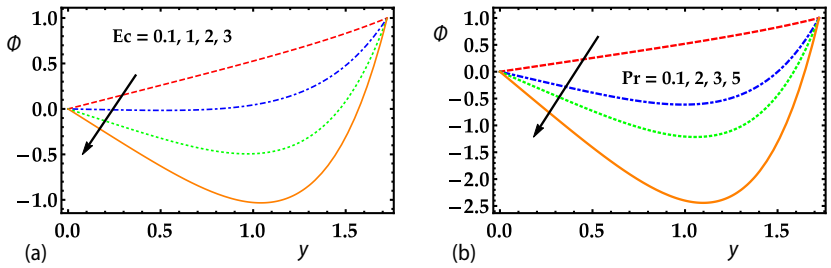

Figure 8. Concentration profile for different values of Ec and Pr, when $\zeta = 0.5$, $\varphi = 0.6$, $\bar{Q} = 0.1$, M = 2, Sc = 2, Sr = 2

The next engrossing part of peristaltic blood flow is trapping which can be observed with the help of streamline. It is the formation of internally circulating trapped bolus that is enclosed by various streamlines. Figure 9 is sketched for different values of Hartmann number. It can be seen from this figure that when the Hartmann number increases, then the magnitude of the trapped bolus reduces slowly whereas the number of the trapped bolus remains constant. It depicts from fig. 10 that due to an effect of Casson fluid parameter, the number of boluses does not change while the size of the trapping bolus decreases.

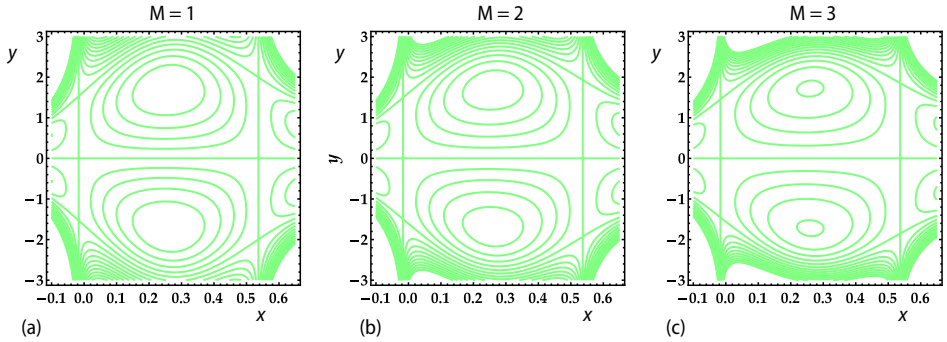

Figure 9. Stream lines for different values of ζ, when $\zeta = 0.5$, $\varphi = 0.6$, $\bar{Q} = 0.1$

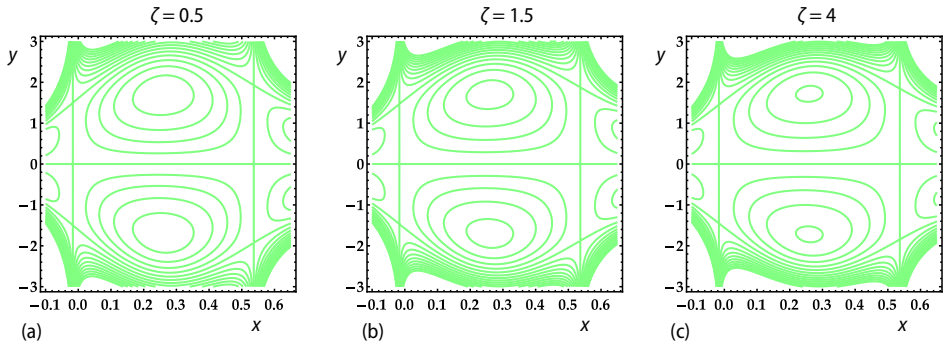

Figure 10. Stream lines for different values of M, when M = 2, $\varphi = 0.6$, $\bar{Q} = 0.1$

Conclusion

In this article, heat and mass transfer analysis are carried out on MHD blood flow of Casson fluid model induced by the peristaltic wave. The governing equations of the flow problem are simplified by taking the assumption of long wavelength and creeping flow regime. The solution of the resulting coupled differential equations have been evaluated analytically and a closed form solutions are obtained. The impact of all the pertinent parameters is demonstrated graphically and mathematically. The major outcomes of the present analysis are as follows.

- Velocity of fluid shows opposite behavior near the walls for Hartmann number and Casson fluid parameter.
- Pressure rise increases due to the increment in Hartmann number, while its behavior is opposite for Casson fluid parameter.
- Temperature profile decreases due to the increment in Eckert number and Prandtl number.

- Concentration distribution increases for higher values of Schmidt number and Soret number.
- The present analysis can also be reduced to a Newtonian fluid by taking $\zeta \to \infty$ as a special case of our study.

Nomenclature

$\tilde{a}$ – wave amplitude, [m]
B_0 – magnetic field, [NmA^{-1}]
$b(\tilde{x})$ – half width of the channel, [m]
$\mathcal{D}$ – mass diffusivity, [m^{2}s^{-1}]
Ec – Eckert number, [–]
F – concentration of the fluid
$\mathcal{K}$ ($\ll 1$) – constant
K_T – thermal diffusion ratio
M – Hartmann number, [–]
Pr – Prandtl number, [–]
P_y – yield stress
$\tilde{p}$ – pressure [Pa]
Q – volume flow rate, [m^{3}s^{-1}]
Re – Reynolds number, [–]
S – stress tensor
Sc – Schmidt number, [–]
Sr – Soret number, [–]
T – temperature of the fluid
$\tilde{t}$ – time, [s]
T_m – mean temperature
$\tilde{u}$, $\tilde{v}$ – axial and transverse velocity, [ms^{-1}]
$\tilde{x}$, $\tilde{y}$ – co-ordinate axis, [m]

Greek Symbols

β – slip parameter
δ – wave number [rad.m1]
ζ – Casson fluid parameter
ζ_0 – specific heat at constant volume, [Jkg^{-1}]
λ – wave length, [m]
μ – dynamic viscosity, [Pas]
μ_b – plastic viscosity
ν – kinematic viscosity, [m^{2}s^{-1}]
ρ – fluid density, [kgm^{-3})
ϕ – amplitude ratio
Ψ – stream function

References

[1] Srivastava, V. P., Saxena, M., Two-Layered Model of Casson Fluid Flow through Stenotic Blood Vessels: Applications to the Cardiovascular System, *J. Biomech.*, *27* (1994), 7, pp. 921-928
[2] Srivastava, V.P., Particle-Fluid Suspension Model of Blood Flow through Stenotic Vessels with Applications, *Int. J. Bio-Med. Comput.*, *38* (1995), 2, pp. 141-154
[3] Srivastava, V. P., Saxena, M., A Two-Fluid Model of Non-Newtonian Blood Flow Induced by Peristaltic Waves, *Rheologica Acta*, *34* (1995), 4, pp. 406-414
[4] Mekheimer, K. S., Peristaltic Flow of Blood under Effect of a Magnetic Field in a Non-Uniform Channels, *Appl. Math. Comput.*, *153* (2004) 3, pp. 763-777
[5] Shapiro, A.H., *et al*., Peristaltic Pumping with Long Wavelength at Low Reynolds Number, *J. Fluid Mech., 37* (1969), 4, pp. 799-825
[6] Srivastava, L. M., Srivastava, V. P., Peristaltic Transport of a Power-Law Fluid: Application to the Ductus Efferentes of the Reproductive Tract, *Rheol. Acta, 27* (1988), 4, pp. 428-433
[7] Gupta, B. B., Seshadri, V., Peristaltic Pumping in Non-Uniform Tubes, *J. Biomech.*, *9* (1976), 2, pp. 105-109
[8] Beg, O. A., *et al*., Homotopy Analysis of Transient Magneto-Bio-Fluid Dynamics of Micropolar Squeeze Film in a Porous Medium: A Model for Magneto-Bio-Rheological Lubrication, *J. Mech. Med. Biol.*, *12* (2012), 3, 1250051
[9] Beg, O. A., *et al*., Comparative Numerical Study of Single-Phase and Two-Phase Models for Bio-Nanofluid Transport Phenomena, *J. Mech. Med. Biol.*, *14* (2014), 1, 1450011
[10] Rashidi, M. M., *et al*., Magnetohydrodynamic Biorheological Transport Phenomena in a Porous Medium: A Simulation of Magnetic Blood Flow Control and Filtration, *Int. J. Numer. Method. Biomed. Eng.*, *27* (2011), 6, pp. 805-821
[11] Akbar, N. S., Heat and Mass Transfer Effects on Carreau Fluid Model for Blood Flow through a Tapered Artery with a Stenosis, *Int. J. Biomath.*, *7* (2014), 1, 1450004
[12] Akbar, N. S., *et al*., Heat Transfer Analysis on Transport of Copper Nanofluids Due to Metachronal Waves of Cilia, *Current Nanosci.*, *10* (2014), 6, pp. 807-815
[13] Nadeem, S., *et al*., Mathematical Model for the Peristaltic Flow of Jeffrey Fluid with Nanoparticles Phenomenon Through a Rectangular Duct, *Appl. Nanosci.*, *4* (2014), 5, pp. 613- 624
[14] Ellahi, R., *et al*., Effects of Heat and Mass Transfer on Peristaltic Flow in a Non-Uniform Rectangular Duct, *Int. J. Heat. Mass. Trans.*, *71* (2014), Apr., pp. 706-719

[15] Reddy, M. G., Makinde, O. D., Magnetohydrodynamic Peristaltic Transport of Jeffrey Nanofluid in an Asymmetric Channel, *J. Mol. Liq., 223* (2016), Nov., pp. 1242-1248
[16] Reddy, M. G., Heat and Mass Transfer on Magnetohydrodynamic Peristaltic Flow in a Porous Medium with Partial Slip, *AEJ – Alexandria Engineering Journal, 55* (2016), June, pp. 1225-1234
[17] Reddy, M. G., Reddy, K. V., Influence of Joule Heating on MHD Peristaltic Flow of a Nanofluid with Compliant Walls, *Procedia Eng., 127* (2015), Dec., pp. 1002-1009
[18] Bhatti, M. M., *et al*., Endoscope Analysis on Peristaltic Blood Flow of Sisko Fluid with Titanium Magneto-Nanoparticles, *Comp. Biol. Med., 78* (2016), Nov., pp. 29-41
[19] Bhatti, M. M., *et al*., Heat Transfer Analysis on Peristaltically Induced Motion of Particle-Fluid Suspension with Variable Viscosity: Clot Blood Model, *Comp. Method. Prog. Biomed., 137* (2016), Dec., pp. 115-124
[20] Bhatti, M. M., *et al*., Study of Variable Magnetic Field on the Peristaltic Flow of Jeffrey Fluid in a Non-Uniform Rectangular Duct Having Compliant Walls, *J. Mol. Liq., 222* (2016), Oct., pp. 101-108
[21] Mekheimer, K. S., Effect of the Induced Magnetic Field on Peristaltic Flow of a Couple Stress Fluid, *Phys. Lett. A.*, *372* (2008), 23, pp. 4271-4278
[22] Mekheimer, K. S., *et al*., Peristatcally Induced MHD Slip Flow in a Porous Medium due to a Surface Acoustic Wavy Wall, *J. Egypt. Math. Soc.*, *22* (2014), 1, pp. 143-151
[23] Rashidi, M. M., *et al*., Numerical Investigation of Magnetic Field Effect on Mixed Convection Heat Transfer of Nanofluid in a Channel with Sinusoidal Walls, *J. Magn. Magn. Mater.*, *401* (2016), Mar., pp. 159-168
[24] Sheikholeslami, M., *et al*., Numerical Investigation of Magnetic Nanofluid Forced Convective Heat Transfer in Existence of Variable Magnetic Field using Two Phase Model, *J. Mol. Liq.*, *212* (2015), Dec., pp. 117-126

Paper submitted: January 2, 2016
Paper revised: September 11, 2016
Paper accepted: October 25, 2016